Phys. Status Solidi C **8**, No. 9, 2927–2930 (2011) / **DOI** 10.1002/pssc.201084062

physica status solidi c
www.pss-c.com
current topics in solid state physics

Water-based sonochemical cleaning in the manufacturing of high-efficiency photovoltaic silicon wafers

A. Nadtochiy[1], A. Podolian[1], O. Korotchenkov[*, 1], J. Schmid[2], E. Kancsar[2], and V. Schlosser[*, 2]

[1] Faculty of Physics, Taras Shevchenko Kyiv National University, Kyiv 01601, Ukraine
[2] Department of Electronic Properties of Materials, Faculty of Physics, University of Vienna, 1090 Wien, Austria

Received 3 October 2010, accepted 4 February 2011
Published online 6 May 2011

Keywords silicon, sonication, photovoltaic

[*] Corresponding authors: e-mail olegk@univ.kiev.ua, Phone: +380 44 526 05 10,
e-mail viktor.schlosser@univie.ac.at, Phone: +43 1 4277 51428, Fax: +43 1 4277 51429
Web: http://www.phys.univ.kiev.ua/genphys/nano_optoel.htm, http://www.univie.ac.at/photovoltaik

We found that organic particle contaminants are effectively removed during ultrasonic cleaning in distilled water, as evidenced by the disappearance of organic-related absorption peaks and remarkable shortening of the surface photovoltage decay transients (SPV). SPV decay transient mappings obtained with a 100-μm spatial resolution (see abstract figure) show that, in multicrystalline Si wafers, the resulting effect on the decay time is markedly non-uniform compared with that observed in crystalline Si, implying the existence of a mechanism associated with the grain boundaries. The data are tentatively interpreted in terms of the wafer hydrogenization, which most probably occur through the grain boundaries. It is assumed that elevated temperatures inside a cavitating bubble may lead to water and bubble gas decomposition, accompanied by a subsequent trapping of the decomposed particulates at the silicon surface. These particulates can then be predominantly incorporated into the grain boundary regions. We suggest that this can be in part due to hydrogen molecules decomposed in water which are mobile in silicon.

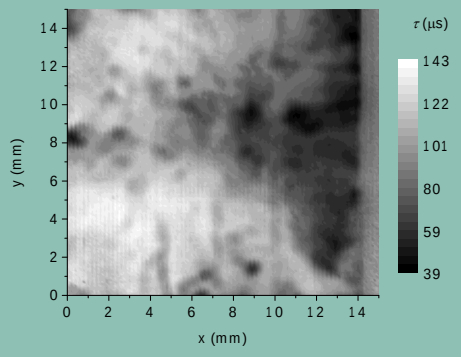

1 Introduction

In recent years, the usage of renewable energy sources like solar cells and panels has increased remarkably. Among installed photovoltaic systems, more than 90% are mono- and polycrystalline silicon cells, which provide the advantages of low cost and large area with relatively high efficiency [1]. Cleaning the surfaces of silicon wafers is one of the most critical operations in device processing technologies [2], in particular, in the photovoltaic industry.

The complete removal of contaminants and the passivation of rechargeable states on the surfaces are very important issues for improving the energy conversion efficiency of Si solar cells which is sensitive to the surface recombination velocity. The point is that more energy is required to remove smaller particles, because it is physically harder to deliver the necessary force to tiny dimensions.

In this context, among other techniques, ultrasonic agitation is widely used to adding energy into the wet cleaning bath. Planar and patterned silicon wafers are routinely cleaned using ultrasonic waves. In this process, the wafers are immersed in a chemically active solution subjected to high power beams of acoustic waves. Sonochemical cleaning has proved to be particular effective, e.g., after pre-oxidation, pre-chemical vapor deposition, pre-epitaxial growth, postash and post-chemical mechanical polishing of Si wafers.

It is commonly believed that the cleaning removes contaminating additives from the wafer surface through acoustic cavitation and acoustic streaming although the physics behind the ultrasonic-induced cleaning process is still not completely understood and the precise cleaning mechanisms are still the subject of debate [3, 4]. The frequency range of the waves used in this process is rather wide, typically in the kHz–MHz range. A combination of induced streaming flows in the cleaning solution, acoustic cavitation, the level of dissolved gases and oscillatory effects are thought to contribute to removing particles and complex organic materials from the wafer surface.

Here, we report the photovoltaic behavior of poly- and monocrystalline Si wafers subjected to a surface cleaning process in ultrasonically agitated distilled water. We concentrate on studying the surface photovoltage (SPV), measuring the variation of surface potential upon illumination.

2 Experimental setups Solar-grade *n*- and *p*-type silicon wafers, crystalline and multicrystalline are sonicated in the distilled water cleaning bath. The setup is shown in Fig. 1. An oscillating voltage with the amplitude of U_0 applied to a Langevin transducer causes it to vibrate, delivering an acoustic power into the water-filled flask with a silicon wafer. The transducer-water resonance frequency (28 kHz) is defined by the water height h. The temperature of the bulk water was kept between 70 and 80 °C during the entire treatment. In the geometry shown in Fig. 1, a cavitation is readily observed at $U_0 \geq 45$ V.

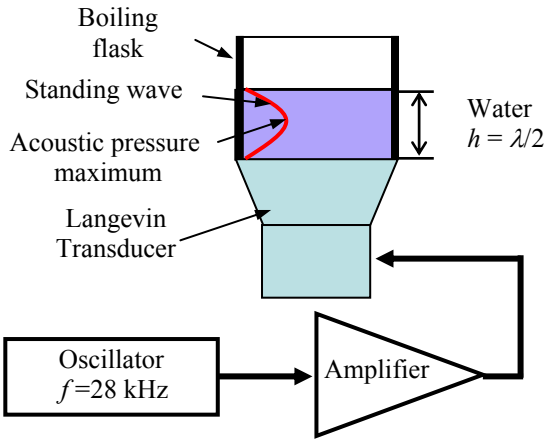

Figure 1 Schematic of the experimental apparatus for sonication of wafers. The water levels up at h, implying the resonance condition, $h = \lambda/2$, is satisfied.

The pressure amplitude P_0 of the incident wave with respect to the wafer surface can be found as

$$P_0 \approx U_0 \rho V \sqrt{\frac{K_t^2 C_t}{M_t}}, \qquad (1)$$

where ρ is the water density, V is the sound velocity in water, M_t is the mass of the transducer, and the electromechanical coupling coefficient K_t is

$$K_t^2 = (\pi f_r / 2 f_a) \cot(\pi f_r / 2 f_a), \qquad (2)$$

with f_r and f_a the resonance and antiresonace frequencies of the transducer. The capacitor C_t represents the shunt capacitance of the transducer. Then the pressure and displacement peak amplitudes are found to be ≈ 3.5 MPa and 13 μm at $U_0 = 225$ V.

SPV transients are measured in the capacitor rrangement [5], and details of our setup are given elsewhere [6]. The scanning SPV apparatus based on the the AC-SPV technique [7] and utilizing a "flying spot" arrangement [8] is used for obtaining SPV decays and spatially-resolved SPV maps. This technique is capable of providing wafer maps of both the photovoltage magnitude and carrier lifetime with a 100-μm spatial resolution.

The Si surface contaminating particles are revealed by a JASCO 5300 FTIR spectrometer.

3 Cleaning efficiency In this work, the cleaning efficiency is characterised by tracing the optical absorption bands of organic particle contaminants. The FTIR absorption spectra resulting from the organic contaminants are marked by several peaks in Fig. 2, with C–CH_3 at 2960 cm^{-1}, –CH_2– at 2920 cm^{-1}, –CH at 2890 cm^{-1} and C–H stretching vibrations [–CH_3 and –$(CH_2)_n$–] at 2850 cm^{-1} [9]. Weighing the data of Fig. 2, it is seen that organic particle contaminants are effectively removed from the wafer surface already at short sonication times (cf. spectra 2 and 3) and the transmission with ultrasonically cleaned surface closely resembles the one taken with a conventionally cleaned wafer (spectra 3 and 1).

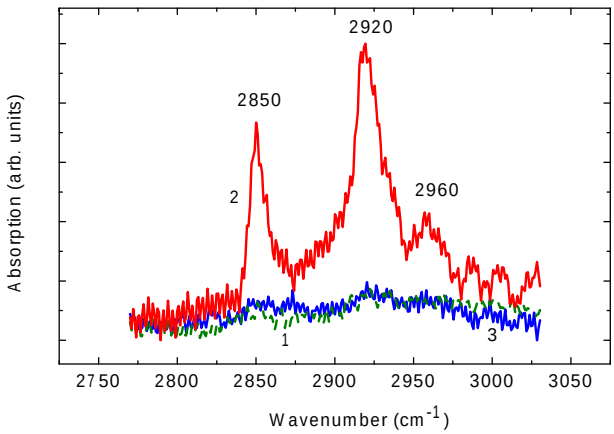

Figure 2 FTIR spectra of a crystalline Si wafer with a surface, conventionally cleaned (1), covered with a thin layer of vaseline mimicking a hydrocarbon contaminant on Si wafers (2) and subsequently cleaned in an ultrasonic bath during 15 min (3).

4 Photovoltaic performance It has already been reported that the wafer sonication, besides the cleaning itself, is accompanied by modifying free carrier migration barriers developed at the interfaces, as deduced from the current-voltage curves, decreasing subsurface resistance towards dislocation displacements, observed by the microhardness decrease, and is capable of accelerating SPV decays [10]. These effects have been tentatively attributed to activation of the air/oxide and oxide/wafer interface dangling bonds. Below we discuss in greater details the comparative photovoltaic performance of monocrystalline and multicrystalline Si wafers.

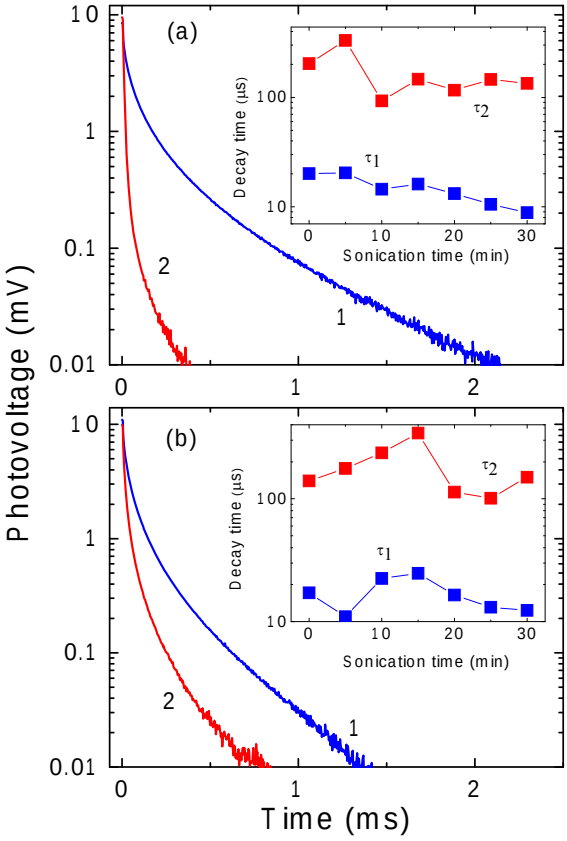

Figure 3 Semi-log plots of the SPV decays on two Si wafers, as-purchased (1) and cleaned in an ultrasonic bath for 25 min (2). Panel (*a*) multicrystalline Si:P, 0.3-3 Ohm·cm, 400-μm thick, panel (*b*) monocrystalline (111) Si:P, 0.5 Ohm·cm, 400-μm thick. Insets: variations of the characteristic decay times τ_1 and τ_2 in the double-exponent fitting of the decay shapes to Eq. (3). The lines in insets are guide to eyes.

The SPV decay data are shown in Fig. 3, illustrating that SPV decays are remarkably affected by the sonication. All the decays are clearly nonexponential shapes exhibiting direct evidence for the involvement of traps and recombination centres in the near subsurface region. Thus, initial rapid SPV decays (at times smaller than 0.2 and 0.5 ms in curves 1 of Fig. 3, *a* and *b*, respectively), when the injected carrier concentrations are large compared with the density of the trapping centers (N_t), are nearly simple exponentials with a time constant τ_1. The final decays (greater than 0.2 and 0.5 μs in curves 1 of Fig. 3, *a* and *b*, respectively), when the carrier concentrations are small compared with N_t are, again, nearly simple exponentials with much greater time constants τ_2 determined by N_t [11].

Fitted to a double-exponent form

$$V = V_1 \exp(-t/\tau_1) + V_2 \exp(-t/\tau_2), \tag{3}$$

the decay shapes exhibit characteristic decay times τ_1 and τ_2 shown in the insets of Fig. 3. It is seen that both the times tend to gradually decrease with increasing the sonication time, so that the decays speed up. Meanwhile, both the τ_1 and τ_2 exhibit a slight increase in monocrystalline wafers at sonication time instants smaller than 15 min [inset in (*b*)], which is not likely reproduced in multicrystalline wafers [inset in (*a*)]. It is also seen in Fig. 3 that the sonication effect on the SPV decay in multicrystalline wafers is greater than that in monocrystalline ones [curves 1 and 2 in (*a*) and (*b*), respectively].

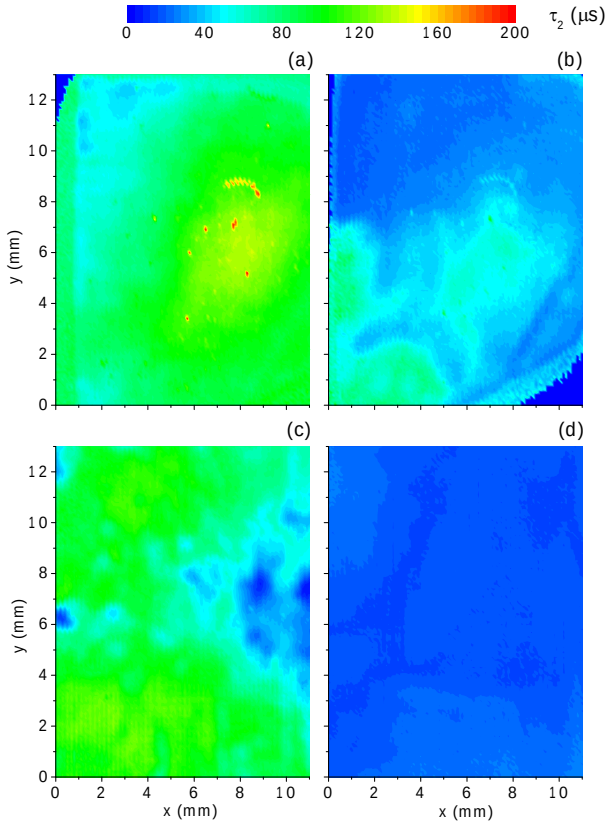

Figure 4 Spatially resolved SPV decay times τ_2 observed on as-purchased [(*a*) and (*c*)] and ultrasonically cleaned [(*b*) and (*d*)] wafers. Cleaning time in (*b*) and (*d*) is 60 min. (*a*) and (*b*) monocrystalline (111) Si:P, (*c*) and (*d*) multicrystalline Si:P. The samples are the same as in Fig. 3.

The difference in the photovoltaic performance of sonicated mono- and multicrystalline wafers is also observed by taking surface distributions of the SPV signal. The SPV decay time τ_2, taken before and after sonication, is mapped for both wafers and the results are shown in Fig. 4. It is seen that, initially, τ_2 for both as-purchased wafers [images (*a*) and (*c*)], observed in, are markedly non-uniform, implying the existence of distributed sites affecting carrier lifetimes.

It is most remarkable that the decay time shortening, already seen in Fig. 3, is accompanied by a remarkable smoothening of the lifetime distribution over the wafer surface [(*b*) compared with (*a*), and (*d*) compared with (*c*) in Fig. 4]. Of further significance is the fact that the smoothening effect is more pronounced in multicrystalline Si wafers compared with monocrystalline Si [(*d*) and (*b*) in Fig. 4, respectively].

It may therefore be suggested that the initial decays (τ_1) are most likely reduced by developing dangling bonds on the bare silicon surface due to a local removal of SiO_2 by cavitating bubbles [10].

Map (*a*) in Fig. 4 implies the existence of microdefects in crystalline Si, acting as recombination centers, which are distributed non-uniformly in the near-surface region of the wafers [12]. Accordingly, the image shows distributed decay times, because τ_2 decreases in the areas of enhanced defect concentrations.

A likely explanation of the smoothening observed in (*b*) relies on the oxygen and hydrogen micro-precipitation of the wafer kept in the water bath. It may therefore be assumed that oxygen and hydrogen precipitation would occur due to their decomposition in water by the presence of local strain fields and elevated temperatures inside a cavitating bubble striking the Si surface.

It is likely that similar changes are also observed in multicrystalline wafers. Meanwhile, based on the fact that the smoothening effect is even more pronounced in multicrystalline Si [(*d*) and (*b*) in Fig. 4], the existence of a competing precipitation mechanism associated with the grain boundaries may be implied. The enhanced smoothening can be tentatively interpreted in terms of the wafer hydrogenization, which most likely occur through the grain boundaries.

It can thus be assumed that elevated temperatures inside a cavitating bubble may lead to water and bubble gas decomposition, accompanied by a subsequent trapping of the decomposed particulates at the silicon surface. These particulates can then be incorporated into the grain boundary regions. We suggest that this can be in part due to hydrogen molecules decomposed in water which are mobile in silicon.

5 Conclusions In summary, it is observed that organic particle contaminants are effectively removed from the Si wafer surfaces in ultrasonically agitated distilled water, which is accompanied by shortening the surface photovoltage decays. This can deteriorate the carrier lifetime and restricts the conversion efficiency of Si solar cells. We found that the observed shortening and its surface distribution are markedly different in mono- and multicrystalline Si wafers. The data are tentatively interpreted in terms of the sonochemical decomposition of the water followed by the wafer hydrogenization, which is enhanced by the grain boundaries in the multicrystalline wafers. Our results contribute in promoting environmentally friendly and non-toxic cleaning steps in manufacturing photovoltaic Si wafers and attempting to improve the photovoltaic performance of solar-grade silicon.

Acknowledgements We gratefully acknowledge the support of the Mitteln des Bundesministeriums für Wissenschaft und Forschung / Die Österreichische Austauschdienst-GmbH (No. UA 09/2009) and Ministry of Education and Science of Ukraine (M/110-2009).

References

[1] M. A. Green, Prog. Photovoltaics **17**, 183 (2009).
[2] S. Wolf and R. N. Tauber, Silicon Processing for the VLSI Era, Vol. 1 (Lattice Press, Sunset Beach CA, 2000).
[3] G. W. Gale and A. A. Busnaina, Particulate Sci. Technol. **13**, 197 (1995).
[4] M. Keswani, S. Raghavan, P. Deymier, and S. Verhaverbeke, Microelectron. Eng. **86**, 132 (2009).
[5] C. Munakata, S. Nishimatsu, N. Honma, and K. Yagi, Jpn. J. Appl. Phys. **23**, 1451 (1984).
[6] A. Podolian, V. Kozachenko, A. Nadtochiy, N. Borovoy, and O. Korotchenkov, J. Appl. Phys. **107**, 093706 (2010).
[7] P. Edelman, J. Lagowski, and L. Jastrzebski, Proc. Mater. Res. Soc. Symp. **261**, 223 (1992).
[8] C. Munakata, K. Yagi, T. Warabisako, M. Nanba, and S. Matsubara, Jpn. J. Appl. Phys. **21**, 624 (1982).
[9] K. Saga and T. Hattori, J. Electrochem. Soc. **143**, 3279 (1996).
[10] A. Nadtochiy, A. Podolian, V. Kuryliuk, A. Kuryliuk, O. Korotchenkov, J. Schmid, and V. Schlosser, in: Proceedings of the 27th International Conference on Microelectronics, Niš, Serbia, 2010 (IEEE, 2010), pp. 261–264.
[11] L. Kronik and Y. Shapira, Surf. Sci. Rep. **37**, 1 (1999).
[12] A. J. R. de Kock, Appl. Phys. Lett. **16**, 100 (1970).

